Temperature and strain measurements with fiber bragg gratings embedded in stainless steel 316

Temperature and Strain Measurements with Fibre Bragg Gratings Embedded in Stainless Steel 316

Dirk Havermann*, Jinesh Mathew, William N. MacPherson, Robert R. J. Maier, Duncan P. Hand

***Abstract*— Single mode optical fibres with thin nickel coatings (outer diameter ~350 µm) are successfully embedded into stainless steel 316 components using bespoke laser based additive manufacturing technology. In our approach we manufacture SS 316 components using Selective Laser Melting, incorporating U-shaped grooves with dimensions suitable to hold nickel coated optical fibers. Coated optical fibers containing fiber Bragg gratings for strain monitoring and temperature sensing are placed in the groove. The embedding is completed by melting subsequent powder layers on top of the fibers. Cross sectional microscopy analysis of the fabricated components, together with analysis of the Bragg gratings behaviour during fabrication indicates a strong substance-to-substance bond between coated fibre and added SS 316 material. Temperature and strain cycling of the embedded sensors demonstrates the ability of gratings to survive the embedding process, and act as sensing elements in harsh environments. In-situ strain and temperature measurements from within the component are demonstrated for high dynamic stress levels and elevated temperatures (< 400 ^{0}C).**

***Index Terms*—laser sintering, laser melting, optical fiber sensors, Bragg gratings, strain sensors, temperature sensors, embedded fiber sensors, stainless steel**

I. Introduction

Embedding of optical fibre sensors into composite materials has been widely reported and has seen extensive use across a wide range of applications for measuring strain and temperature from within the components creating intelligent structures. In-situ measurements offer potential to enhance asset management, including lifetime monitoring, and the safe use of components closer to their design limits of mechanical stability [1]. Predominately, the embedment of fibre optic sensors has been demonstrated either in structures manufactured from composite materials [2] and plastics [3] or by utilising epoxy adhesion for bonding to metal materials[4], all of which are systems which limit the usable temperature range to temperatures below maximum 350 °C.

The aim of the research presented in this paper is to extend the benefits of embedded fibre optic sensing to include systems composed of metallic materials with high melting temperatures, such as widely used stainless steel alloys.

Manuscript received September 09, 2014; revised 24-10-2014; accepted 26-10-2014. Date of publication xxx xx, xxxx; date of current version 30-10-2014

This work was supported in part by the EPSRC and a EU project under Grant 310279.The authors are with the Applied Optics and Photonics Group, Institute of Photonics and Quantum Sciences, SUPA, Heriot-Watt University, Edinburgh, EH14 4AS, UK e-mail: dh108@hw.ac.uk

In-situ measurements of strain and temperature in environments with temperatures exceeding 1000 °C are highly desirable for energy and aerospace applications. Difficulties arise from achieving reliable bonding between glass and metal at these elevated temperatures [5] and a particular challenge arises from the relatively low annealing point of fused silica (~1100 °C [6] which is low compared to the melting point for most stainless steel alloys (typically around 1450 °C [7]).

Few concepts for embedding Fibre Bragg gratings (FBG) into metal components suitable for high temperature applications have been reported previously. Commonly used is the approach of protecting the optical fibres with metal jackets prior to encapsulation. These metal jackets are typically applied by low temperature processes such as electro-less plating [8] or a mixture of electro-plating and magnetron sputtering [9]. Subsequently, the jacketed fibres are encapsulated either by using low temperature manufacturing processes such as ultrasonic consolidation [10] or by using brazing [11] and high temperature additive manufacturing processes such as fused deposition modelling [9]. Low temperature embedding processes inherently limit the range of applications that the final component may be used in and the high temperature approach described by Li [9] requires very thick nickel fibre jackets which significantly change the final component mechanical and material properties. Ideally we desire to be able to embed fibre sensors into a high temperature build component, without compromising the final physical properties of the system.

In this paper we demonstrate the feasibility of embedding fibre Bragg gratings into stainless steel 316 (SS 316) components by using powder bed based Selective Laser Melting (SLM). The excellent beam quality of commercially available laser systems allows power delivery with small spot sizes of a few tens of micro-meters in diameter. Small spot sizes are beneficial for this application because they lead to smaller melt pools and therefore to less heat conduction and minimised heat affected zones into the surrounding material [12]. Melt pool temperatures in steel sintering processes are typically several hundred degrees above the steel melting point to ensure that the localized melt zone extends beyond the focal volume of the laser beam to facilitate partial re-melting of the neighbouring materials and hence help to achieve a crack free solid component [13]. High brightness laser melting processes allow very precise spatial and temporal control of the energy input into the process zone, allowing good control over the melt pool in vicinity of the embedded optical fibres to prevent inflicting structural damage to the fibre. The amount of energy transferred into the fiber is

minimised, which protects the integrity of the fibre and also reduces the thickness of the jacket required to protect the fibre during the embedding process. This in turn minimises the structural intrusion of the manufactured component created by the incorporation of the sensor element.

SS 316 is not an ideal material suitable for long-term high temperature applications, however, here it has been chosen as a suitable stand-in material to demonstrate the feasibility of our concept. SS 316 has been chosen due to its easy availability, low cost, significantly simplified handling and lower health and safety risks compared to more suitable high temperature materials. In the future, SS 316 will be replaced with a nickel based super-alloy, more suitable for applications at very high temperatures. Therefore, long-term (months; years) stability tests or occurrence of fatigue of the SS 316 components are not addressed in this paper.

We demonstrated embedment of optical fibres into SS 316 components and subsequent in-situ temperature sensing in the earlier conference paper presented at OFS-23 in Santander (June 2014) [14]. This extended paper provides a more detailed description of the embedding process and will assess the repeatability of the embedding process. Additionally, we verify the delamination of glass and metal at high temperatures in the conference paper. Also, we present results for in-situ elastic strain testing with embedded fibre Bragg gratings embedded into stainless steel 316.

II. Embedding optical fibres in Stainless Steel

To embed fused silica fibres in stainless steel we require a metal jacket to protect the fibre and to form a bond with the steel surrounding. This bond is essential to transfer strain and temperature changes of the metal component into the optical fibre when measuring these changes. We use a combination of RF sputtering of chromium to act as an adhesion layer and a conducting path for subsequent electroplating of nickel using a nickel-sulphamate bath. Both coating materials, chromium and nickel are common constituents of stainless steel alloys and form easily bonds with steel alloys. We have developed a process based upon the recipe described by Li [9] however the thickness of protective coatings applied in our work are more than 5 times thinner and hence have a reduced impact on the structural integrity of the finished component.

In our experiments, the final nickel coating surface is smooth and without visible imperfections. The outer diameter of the coated fibre depends upon the duration of the electroplating process and increases typically in the range of 30-70 $\mu m \cdot hr^{-1}$ for current densities in the range of 8-12 A dm^{-2}. When coating fibres containing FBGs the Bragg wavelength after nickel coating is typically shifted by about 0.5 nm to short wavelengths due to the temperature of the plating bath (50 °C). Differences in thermal expansion of glass and nickel yield compression of the grating at ambient temperatures.

Coated fibres are then embedded utilising Selective Laser Melting technology, which allows building of components layer by layer. Our approach for fibre embedding is divided in three steps (Figure 1). Firstly, material is added on stainless steel (SS-316) substrates (50×20×1.2 mm^3) by SLM.

A 'U'-shaped groove is produced during the SLM process that is tailored to the dimension of the coated optical fibres. The parameters of the SLM process have been selected such that for each layer the re-melt depth into the substrate is in excess of 100 % of the topmost layer thickness, eliminating porosity and guaranteeing proper bonding between supporting layers. Energy input of the SLM process is minimised by only applying thin layers of about 30 µm thickness, also enhancing precision of the U-shaped groove. Metal jacketed fibres are inserted into the groove. The fibre is held in alignment using a mount that applies a small amount of pre-tension to the fibre to help mitigate against movement of the fibre due to thermally induced deformation during the subsequent SLM process. The fibres are clamped fixed on one side and on the other side a free floating weight (100g) is applying a tensile load to the fibre. Following this attachment, the fibres are encapsulated by continuing the SLM process on top of the fibres. In the encapsulation stage the powder is melted in a controlled manner using a laser beam that is scanned perpendicular to the direction of the fibre. In this way, the powder bonds to itself, forming a homogenous solid layer, and it also bonds to the substrate and the nickel coated fibre. Further applications of powder layers and laser processing allow a solid metal component to be fabricated with layer-by-layer control of features.

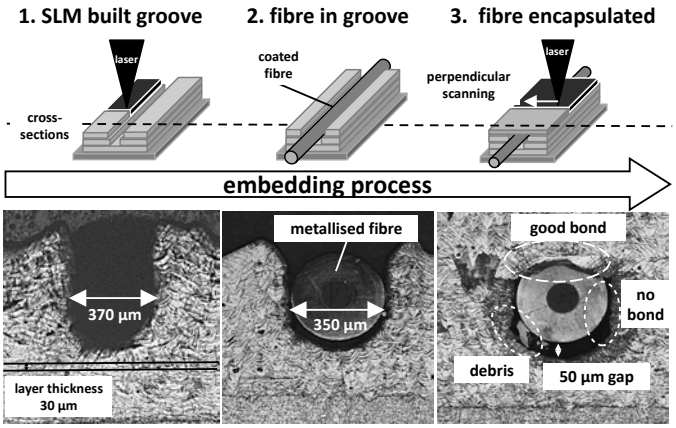

Figure 1.Embedding process in three steps: Building the 'U'-shaped groove with SLM on SS 316 substrates (left), inserting Nickel coated optical fibre in the groove (middle) and final encapsulation by continuing SLM process (right)

Significant effort must be made to select the correct laser properties to ensure melting the powder material without damaging the coated optical fibres. A cross section of a fibre encapsulated in this manner is shown in Figure 1 (right). In this example about 30 % of the circumference of the nickel coated fibre is well bonded to the surrounding steel environment. Imperfections in encapsulation remain on the sides and underneath-side of the coated fibre. Also, debris remaining in the groove is adding to the gaps on the underside. Further development in the delivery of the sintering laser power is required to develop an approach to eliminate these undesirable imperfections.

In this manner, nickel coated optical SMF-28 fibres can be embedded while preserving their mechanical integrity during the embedding process. Figure 2 displays these losses for

nickel coated SMF-28 fibres for various coating thicknesses. Typically, for coating thicknesses of about 350 to 500 µm, these losses are reduced with increased coating thickness and are in the range in the range of 10 to 30 % for an embedding length of 3 cm. With coating thicknesses >500 µm losses are less than 10 %. Analysis of samples suggests that for coating thicknesses less than 350 µm the heat input during the encapsulation process is sufficient to cause complete melting of the coating. Surface tensions cause contraction of the molten coating material (Figure 2), leading to exposure of the optical fibre to the incident laser radiation and therefore ultimately causing structural damage of the optical fibres.

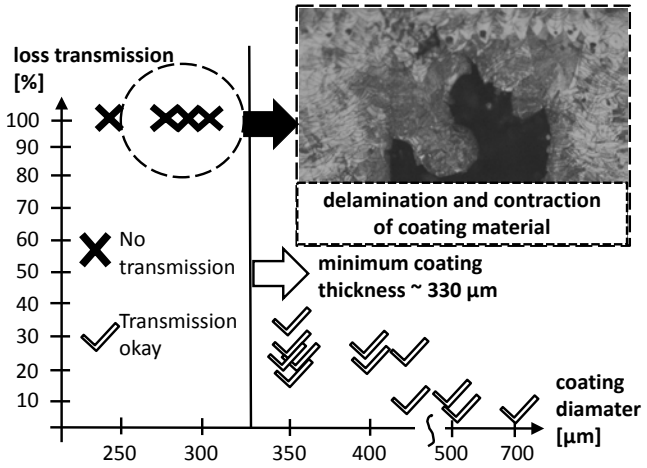

Figure 2. Plot of losses in transmission over thickness of nickel coatings for experiments conducted. Cross-section of fibre with delaminated coating material.

During embedding, the majority of the losses occur during the sintering of the 1st layer above the fibre. Figure 3 displays the transmission spectrum of an embedded FBG before and after the 1st layer of added material. Subsequent layers only cause a small increase in loss, and after the 5th layer, no further loss or changes in transmission are observed. Preliminary results also indicate that losses in transmission can be reduced changing the scanning pattern of the SLM process from e.g. perpendicular scanning to scanning parallel to the optical fibre.

III. Embedding Fibre Bragg Gratings

For in-situ temperature measurements fibre Bragg gratings written into SMF-28 fibres were metal jacketed and encapsulated into stainless steel, utilizing the process described above. After RF sputtering and nickel electro-plating the fibre outer diameter was 350 µm and the peak reflectivity centred on 1550 nm before coating shifted by about 0.5 nm to 1549.5 nm after coating. Figure 3 illustrates the transmission spectrum of one of the FBG after coating, but before embedding, the transmission after the 1st applied layer by SLM and also the transmission after adding more than 20 layers. The spectral width (FWHM) of the grating before embedding was 663 pm. After applying the first layer the grating width almost doubles to 1.183 nm and the peak is centred on 1549.1 nm, which accounts for a wavelength shift of 0.43 nm. It is evident that the embedding process results in residual compression being imposed on the grating affecting the position and width of the reflection spectra.

Point loads, depending on the scanning parameter of the SLM process, cause inhomogeneous strain distribution along the optical fibre and lead to losses in transmission through micro bending. Also, these point loads lead to perturbations in the FBG itself and therefore a broader spectral width. When changing polarisation of the injected light the spectral characteristics at the peak wavelength slightly change indicating the occurrence of Birefringence due to non-axisymmetric tensile stresses in the fiber cross-sectional plane.

The grating is under compressive load caused by significant differences in thermal expansion coefficients (ΔCTE) of SS 316 and fused silica (ΔCTE ~ 15×10^{-6} K^{-1}). The ambient temperature of the specimen significantly increases during the embedding process such that the steel expands much more rapidly compared to the optical fibre. During embedding, the laser melting process produces a substance-to-substance bond between the nickel coating and the surrounding SS 316 material. After embedding, the nickel follows temperature changes with the thermal expansion coefficient of steel due to the strong adhesion to the larger steel structure. When cooling the specimen, both the coated fibre and the steel contract with the much higher rate of contraction for SS 316 yielding thermal residual stress and ultimately leading to longitudinally compressive stress of the FBG at ambient temperatures.

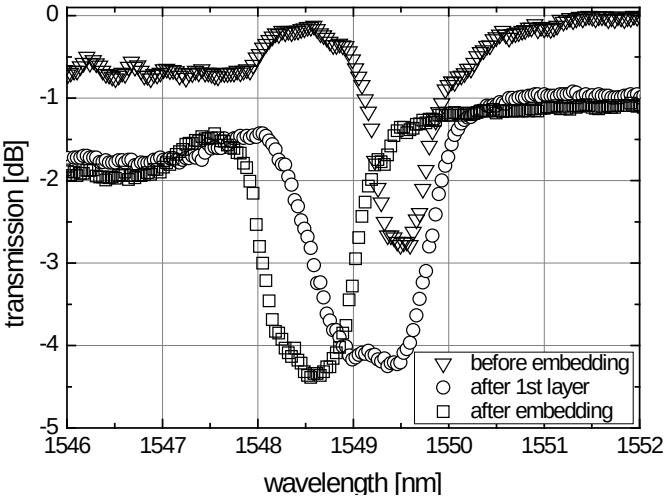

Figure 3. Spectral transmission of nickel coated FBG before, after 1st applied layer and once after embedding is complete.

During the continuing SLM process the grating peak shifts further to shorter wavelengths and reaches its final position at 1458.54 nm after adding the 5th layer. Subsequent re-melting of the first applied layer smooth the inhomogeneous strain levels induced by the first layer leading to a narrower grating width of 920 pm. Additionally, re-melting of the bond between coating and steel leads to further compressive stress. However, after a few layers, enough material has been added such that the re-melting depth is not sufficient to melt the substance-to-substance bond between fibre coating and added steel.

IV. In-situ temperature sensing

Embedded FBGs are placed in a high temperature (1200 °C) tube furnace (CARBOLITE) for temperature cycling, to assess their suitability as temperature sensors. Test components are packaged together with K-type thermocouples. The thermocouple is positioned in close proximity to the specimen to minimise any temperature difference between the thermocouple and test component. A Micron Optic interrogator system (SM 125) is being used to interrogate the FBGs. LabVIEW software is used to record and correlate data from both, interrogator and thermocouple. A 2nd order polynomial peak fit is applied to the spectrum for accurate determination of the location of the Bragg peak.

Initially, the furnace is programmed to cycle between 100 °C and 450 °C with a slow ramp rate (1 °K/min) to allow the heat to be distributed homogenously inside the furnace. For comparison reasons, an embedded FBG in SS 316 and a bare non coated optical fibre with similar FBG are tested with this temperature profile. Figure 4 displays the changes in Bragg wavelengths over the temperatures measured by thermocouples for both components, 10 cycles each, after initial annealing effects of the gratings had vanished. The bare fibre follows temperature changes with about 10.7 pm K^{-1} in average and the embedded FBG with about 31.7 pm K^{-1}.

The increased temperature sensitivity of the embedded FBG of 31.7 pm K^{-1} corresponds to a thermal expansion coefficient (CTE) of 15.8×10-6 K^{-1}, which is close to the CTE of stainless steel 316 (16.2×10-6 K^{-1}). The axial and lateral stress between fibre and its metal coating linearly increases with higher temperatures due to significant differences in CTE between silica (4.9×10-7 K^{-1}) and steel. At temperatures of 400 °C the stress level induced by different CTEs equals straining the optical fibre axial by about 6 mε (Figure 4). If the temperature is increased further (Figure 5; left) the induced axial stress levels as well as lateral stress levels become too large, leading to delamination of the coating material and rapid relaxation of the strained optical fibre.

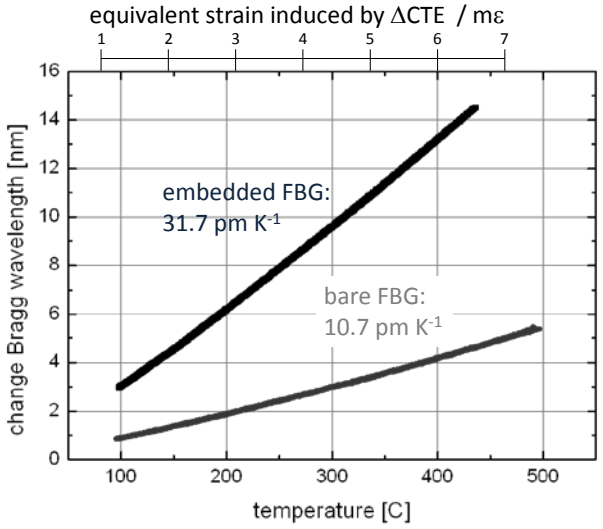

Figure 4. Change in Bragg wavelength due to temperature changes for embedded FBG in SS 316 and bare uncoated FBG.

The rapid relaxation of the fibre causes a discontinuity in the response to temperature changes, indicated by a sudden drop in Bragg wavelength of about 2 nm. Subsequently, when observing these discontinuities and further heating is applied, the temperature sensitivity of the embedded FBG is reduced to about ~10 pm K^{-1}, which is similar to the values of a bare FBG. This decreased temperature sensitivity is evidence that at that particular time no bond between fibre and metal surrounding exists. If the specimen is then cooled down, the observed sensitivity recovers to 31.7 pm K^{-1}, indicating the fibre is again bonded to the metal.

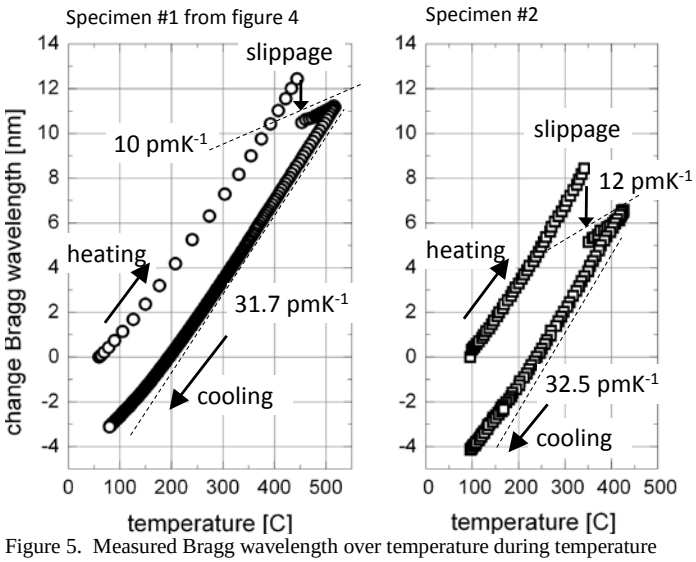

Figure 5. Measured Bragg wavelength over temperature during temperature cycling for two samples where slippage occurred.

After applying this temperature treatment, the Bragg wavelength at ambient temperature has shifted by about 3.5 nm to shorter wavelengths, indicating that the grating is under further longitudinal compressive stress. In subsequent temperature cycles, after initial annealing effects vanished and temperatures do not exceed the temperatures of previous cycles, the gratings response is stabilized. When increasing the temperature to higher levels, the fibre is strained again until the occurring stresses overcome the bonding mechanism and further discontinuities are observed.

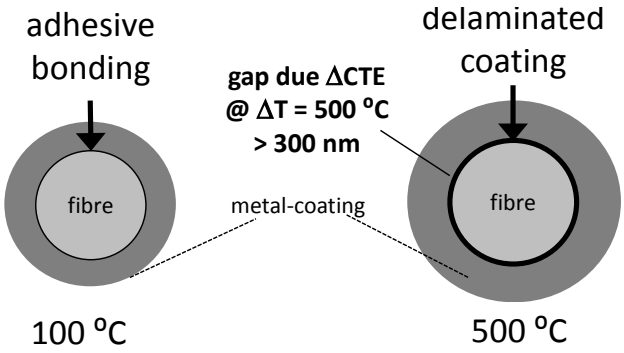

Figure 6. Schematic visualisation of the delamination of the nickel coating from the silica fibre. Due to different CTE, estimates indicate gaps of more than 300 nm between fibre and metal coating.

Repeating these measurements with similarly embedded FBGs (e.g. Figure 5; right) indicates that this phenomenon occurs at

temperatures above 350 ^{0}C, whereby the delamination displayed in Figure 5 (right) was observed at the lowest temperature so far. At these temperatures, when bonding ultimately fails, the fibre detaches from the metal environment with its strain spontaneously relaxing, resulting in an immediate drop in Bragg wavelength. The estimated size of the gap between nickel coating and silica fibre due to differences in CTE at 500 ^{0}C is more than 300 nm (Figure 6). At the moment we can only speculate about the exact point when delamination occurs but we think handling of the fibres before coating (stripping, cleaning etc.) will definitely have an impact on the endurable stresses of the glass-metal bond.

The significantly reduced response of the FBG peak position to temperature, dropping from ~32 pm K^{-1} to 11 pm K^{-1}, which is the nascent response of a free FBG, after discontinuities occurred seconds our argument of delamination of metal and glass. When cooling the specimen, the grating instantaneously follows the steel's contraction again. Due to the increased compression, cycling between similar temperatures in subsequent treatments should not cause any discontinuities since the fibre is under longitudinal compressive stress and no tensile stresses occur at the glass-metal interface.

V. Strain Sensing

For the purpose of strain testing another FBG was embedded into SS 316 in the same manner as described above. The resulting influences on the FBG spectral response were similar to that described earlier for the sample used for temperature sensing. The new sample with the embedded FBG (Figure 7) was clamped in a tensile testing machine. Interrogation of the grating is conducted as with the temperature sensing.

The actual strain is measured by an extensometer (Instron "axial clip-on" Type 2630) clamped onto the sample. Strain is applied by moving one clamping mechanism of the tensile testing machine at very slow speeds (1 µm min^{-1}). The load cell of the tensile testing machine provides corresponding values for the applied force.

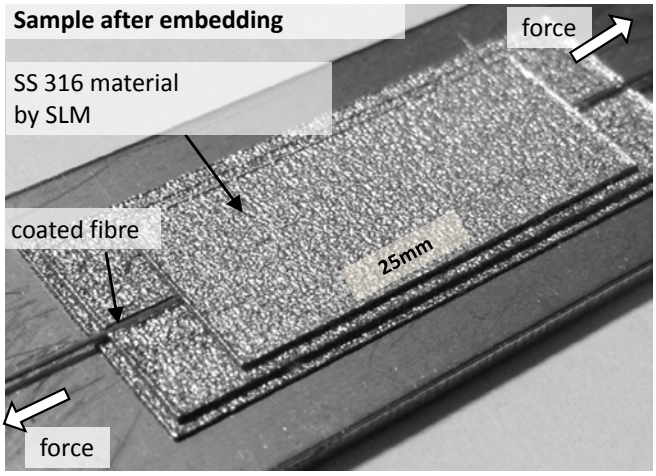

Figure 7. Image of steel sample with embedded FBG for strain testing.

A maximum load of 2 kN was chosen which is equivalent to a stress level in the coupon of about 100 N mm^{-2}. This corresponds to about 50 % Yield Strength of SS 316. When reaching the maximum load of 2 kN, the tensile testing machine was set to reverse to relive the strain at the same speed. To compensate for temperature sensitivity of the embedded FBG, a thermocouple was glued onto the test coupon and the temperature measured. Subsequently the FBG response was compensated for ambient temperature changes. LabVIEW software is used to record and correlate both data streams from FBG interrogation and tensile testing machine. Recorded data for measured strain and interrogated FBG covering about an day after initial plastic deformation and slippage in the clamping mechanism had eased are displayed in Figure 8.

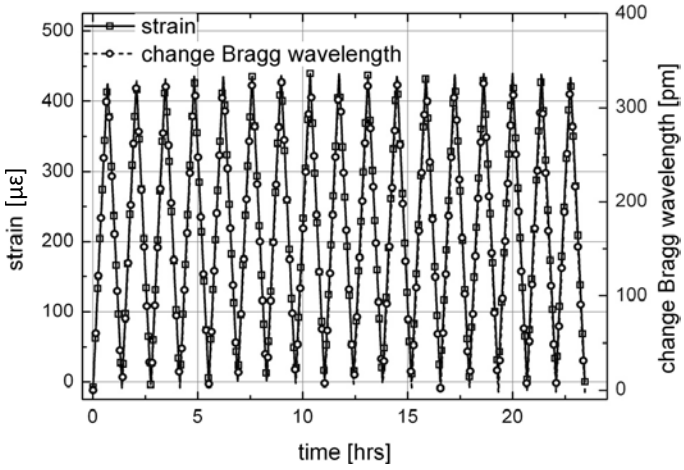

Figure 8: Plot of strain and change in Bragg wavelength over time

In this manner, the sample is strain tested in an elastic dynamic mode for more than 3 weeks where apart from the first initial cycles no permanent plastic deformation of the component is observed. The temperature compensated change in Bragg wavelength over applied strain for one cycle of straining and relieving after more than 500 cycles is illustrated in Figure 9.

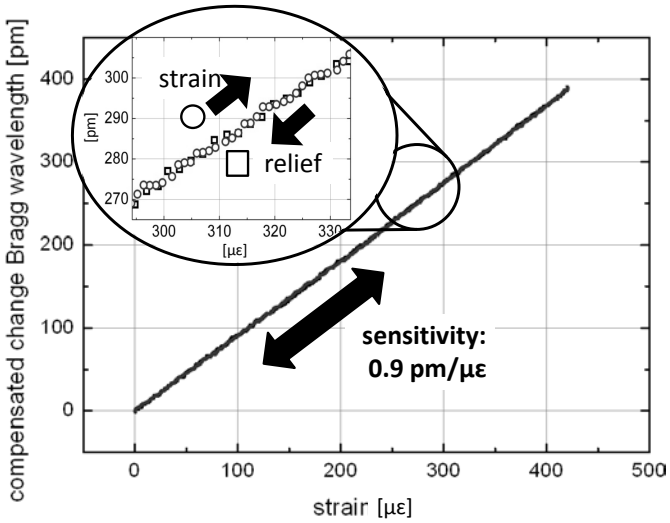

Figure 9: Plot of temperature compensated change in Bragg wavelength over changes in strain level for one strain cycle.

Linear fitting to the plot in Figure 9 determines the sensitivity of the embedded FBG to strain of about 0.92 pm $\mu\varepsilon^{-1}$ which is less than the 1.20 pm $\mu\varepsilon^{-1}$ predicted for a bare SMF-28 fibre with similar grating properties. This deviation is to some extend explainable through axial misalignment between the plane where the fibre is located and the plane the axial stress is induced. Residual distribution of the measured Bragg wavelength about this fit is spread within a band of $\pm$ 3 pm $\mu\varepsilon^{-1}$. For individual cycles of straining and relieving, data sets are within 2 pm of each other, indicating the reliability of the conducted measurements.

However, it is worth noting, that the induced strain levels in the tensile testing machine due to the physical properties of SS 316 are a factor of 10 smaller compared to the axial strain levels that occur due to the different CTE of glass and metal during the temperature measurements.

VI. Discussion & Conclusion

Embedded gratings hold great promise for structural temperature and strain monitoring. Due to the occurring induced stresses at elevated temperatures, the observations of the discontinuities in the data are a cause of concern for implementation as practical sensors. Our experiments show that at higher temperatures the differential thermal expansion between the metals and glass is sufficient to cause delamination between silica fibre and metal. The bond between glass and the RF sputtered Chromium is thought to be only of adhesive nature [5]. The axial strain induced due to different thermal expansion at 400·°C equals stresses of more than 400 N mm^{-2}. This axial stress is radially transferred into the fibre by the glass-metal bond and ultimately, these radially stresses will overcome the adhesive bonding mechanism. The resulting slippage results from the observed discontinuities in the Bragg gratings response during temperature cycling.

This paper demonstrates the feasibility of embedding fibre Bragg gratings coated with comparatively thin metal jackets (~350 µm diameter) into stainless steel components. The gratings optical properties are maintained during the embedding process, enabling in-situ measurements of strain and temperature changes. Repeatable strain measurements with high dynamic stress levels have been demonstrated. For temperature sensing applications at elevated temperatures the occurring issues with the glass metal bonding have to be overcome. Possible solutions for tackling this issue involve embedding of fibres with varying outer diameter for better strain transfer between metal and fibre or adding metal jackets by considering different coating techniques to increase the thermally induced residual strain by the coating process.

References

[1] M. Majumder, T. K. Gangopadhyay, A. K. Chakraborty, K. Dasgupta, and D. K. Bhattacharya, “Fibre Bragg gratings in structural health monitoring—Present status and applications," *Sensors and Actuators A: Physical*, vol. 147, no. 1, pp. 150-164, 2008.

[2] K. S. C. Kuang, R. Kenny, M. P. Whelan, W. J. Cantwell, and P. R. Chalker, “Embedded fibre Bragg grating sensors in advanced composite materials," *Composites Science and Technology*, vol. 61, no. 10, pp. 1379-1387, 2001.

[3] R. R. J. Maier, W. N. MacPherson, J. S. Barton, M. Carne, M. Swan, J. N. Sharma, S. K. Futter, D. A. Knox, B. J. S. Jones, and S. McCulloch, “Embedded Fiber Optic Sensors Within Additive Layer Manufactured Components," *Ieee Sensors Journal*, vol. 13, no. 3, Mar, 2013.

[4] T. K. M. Gangopadhyay, C. Paul; Bjerkan, Leif, "Fiber-optic sensor for real-time monitoring of temperature on high voltage (400KV) power transmission lines." pp. M-1-4.

[5] V. C. Guilbaud-Massereau, A.; Machet, J., “Study and improvement of the adhesion of chromium thin films," *Thin Solid Films*, vol. 258, pp. 8, 1994.

[6] Heraeus-Quarzglas. "*Thermal properties of fused silica*," http://heraeus-quarzglas.com/en/quarzglas/thermalproperties/Thermal_properties.aspx [Accessed: October, 2014].

[7] P. Marshall, "*Austenitic stainless steels : microstructure and mechanical properties*, London: Elsevier Applied Science, 1984.

[8] Y. Li, Z. Hua, F. Yan, and P. Gang, “Metal coating of fiber Bragg grating and the temperature sensing character after metallization," *Optical Fiber Technology*, vol. 15, no. 4, pp. 391-397, 2009.

[9] X. Li, “Embedded Sensors in Layered Manufacturing,” PhD, Mechanical Enginnering, Stanford University, Stanford, 2001.

[10] Y. Li, W. Liu, Y. Feng, and H. Zhang, “Ultrasonic embedding of nickel-coated fiber Bragg grating in aluminum and associated sensing characteristics," *Optical Fiber Technology*, vol. 18, no. 1, pp. 7-13, 2012.

[11] S. Sandlin, T. Kinnunen, J. Ramo, and M. Sillanpaa, “A simple method for metal re-coating of optical fibre Bragg gratings," *Surface and Coatings Technology*, vol. 201, no. 6, pp. 3061-3065, 2006.

[12] I. Yadroitsev, A. Gusarov, I. Yadroitsava, and I. Smurov, “Single track formation in selective laser melting of metal powders," *Journal of Materials Processing Technology*, vol. 210, no. 12, pp. 1624-1631, 2010.

[13] M. Rombouts, J. P. Kruth, L. Froyen, and P. Mercelis, “Fundamentals of Selective Laser Melting of alloyed steel powders," *CIRP Annals - Manufacturing Technology*, vol. 55, no. 1, pp. 187-192, 2006.

[14] D. Havermann, W. N. MacPherson, R. R. J. Maier, and D. P. Hand, “In-situ measurements with fibre Bragg gratings embedded in stainless steel," in 23rd International Conference on Optical Fibre Sensors,, Santander, Spain, 2013, pp. 4.